Plasma Sources Sci. Technol. **18** (2009) 014012 (12pp) doi:10.1088/0963-0252/18/1/014012

Modeling Langmuir probes in multi-component plasmas

R F Fernsler

Plasma Physics Division, Naval Research Laboratory, Washington, DC, USA

Received 17 July 2008, in final form 22 August 2008
Published 14 November 2008
Online at stacks.iop.org/PSST/18/014012

Abstract

Langmuir probes are conceptually simple devices and have long been the primary diagnostic for plasmas, but interpreting the output is rarely straightforward, even in plasmas consisting of Maxwellian electrons and a single ion species. The problem is worse yet in more complicated plasmas where theoretical calculations are lacking. To help interpret probe data, this work presents a numerical scheme capable of modeling spherical and cylindrical probes in plasmas containing any number of charged species, positive or negative. The scheme is based on solving the derivative of Poisson's equation as an initial-value problem rather than solving Poisson's equation as a boundary-value problem. Because the new equation is linear in the electric field, stable solutions are possible. The same approach can be used with other nonlinear ordinary differential equations as well, but in most cases the initial conditions must be adjusted until the original boundary conditions are satisfied. Fortunately, this difficulty is easily circumvented for certain types of problems, including Langmuir probes. Accordingly, Langmuir probes can be modeled quickly and easily, even in plasmas containing multiple ion species and multi-temperature electrons. Examples are given for electropositive plasmas, electronegative plasmas, and two-temperature electrons.

(Some figures in this article are in colour only in the electronic version)

1. Introduction

Langmuir probes offer a simple and convenient means for determining the local properties of plasmas. However, because all the charged species within the plasma contribute, the probe current I_p has a complicated dependence on the applied voltage ϕ_o. Interpreting the probe characteristic $I_p(\phi_o)$ is therefore difficult, and conclusions drawn from different portions of the characteristic often disagree [1–8]. Indeed, even the optimal probe shape is in dispute [5, 8, 10–15]. Theoretical calculations of $I_p(\phi_o)$ are equally challenging, even for plasmas containing Maxwellian electrons and a single ion species [9–13]. Look-up tables [10], algebraic fits [3, 9, 12, 14] and graphical solutions [10, 12] are common. Although some work has been done on two-temperature electrons [16] and simple electronegative plasmas [17], the general plasma case has not been treated, mainly because of the difficulty in solving Poisson's equation.

The goal of this work is to present a numerical scheme which enables the general researcher to compute $I_p(\phi_o)$ quickly and easily for plasmas containing any number or type of charged species. The simplest Langmuir-probe model is the radial-motion theory developed by Allen, Boyd and Reynolds (ABR) [18] for cold ions and negatively biased probes. This theory works well in cold, weakly ionized gases at low pressure, because the electron temperature T_e must then be high ($\geqslant$1 eV) to ionize the gas while collisions with molecules keep the ion temperature close to the gas temperature, $T_i \simeq T_g \ll T_e$. Near a small probe the ions are effectively collisionless, so positive ions strike the probe with an energy $|e\phi_o| \gg T_i$. The temperature T_i of the positive ions then has little effect on the probe current I_p. To treat warm (monoenergetic) positive ions, the orbital-motion theory developed by Bernstein and Rabinowitz (BR) [19] and later corrected by Chen [12] can be used instead. Both theories can be modified to allow for multiple ion species, and both can be attacked as described below. ABR theory is used in this work for simplicity, and readers uninterested in the derivation can skip to section 5 for the final equations.

This work differs from past efforts in that the derivative of Poisson's equation is used in place of Poisson's equation [20]. Benilov [21] and Kono [22] took the same approach with other plasma problems, and Fernsler [23] generalized the approach in both kinetic and fluid forms. However, Fernsler

 © 2009 IOP Publishing Ltd Printed in the UK

concentrated on the quasineutral regions of the plasma only. The numerical approach outlined here can be used with other nonlinear, ordinary differential equations (ODEs) as well, but the overall utility must be assessed on a case-by-case basis.

2. Numerical scheme

In the ABR and BR theories, the plasma charge density ρ is a function of the local electrostatic potential ϕ and the distance r from the probe. Poisson's equation then reduces to a second-order, nonlinear ODE for $\phi(r)$. The potential $\phi(r)$ approaches zero far from the probe and equals the bias voltage ϕ_o at the probe surface r_o. However, because ρ decays faster than ϕ at large r, an ever-finer spatial scale is needed to maintain numerical stability. Previous researchers [10, 12, 13, 17, 18] dealt with this problem by restricting the range covered in r, but the outer boundary condition is then imprecise [10, 17].

In both theories Poisson's equation is a nonlinear, one-dimensional boundary-value problem of the form

$$L_1(\phi) = -4\pi\rho(r, \phi), \tag{1}$$

where L_1 is a differential operator in r. When the inhomogeneous term $\rho(r, \phi)$ is linear in ϕ, the dependent variable $\phi(r)$ can be determined using matrix inversion or similar techniques. But when $\rho(r, \phi)$ is nonlinear, other methods must be used.

To recast equation (1) in a linear form, take its derivative:

$$-\frac{\mathrm{d}}{\mathrm{d}r}L_1(\phi) \equiv L_2(E) = k_s^2 E - Q_c. \tag{2}$$

Here L_2 is a differential operator of the same order as L_1, and

$$E = -\frac{\mathrm{d}\phi}{\mathrm{d}r}, \tag{3}$$

$$k_s^2(r, \phi) = -4\pi\frac{\partial\rho}{\partial\phi} \tag{4}$$

and

$$Q_c(r, \phi) = -4\pi\frac{\partial\rho}{\partial r}. \tag{5}$$

For convenience, the signs and terminology are the same as in [23]. As noted there, equation (2) applies only when ϕ depends on a single variable r. This excludes partial differential equations, including Poisson's equation in two or more dimensions.

Linearization offers two distinct, numerical advantages. First, the troublesome term ρ splits into two parts, one of which is linear. Treated as an initial-value problem, equation (2) can then be solved implicitly, explicitly or semi-implicitly. This property is especially useful when ρ approaches zero faster than E. And second, numerical stability is now easy to assess. For further discussion and generalization, see appendices A and B.

3. Initial conditions and model assumptions

Because the new ODE is one order higher than the original equation, one or more additional initial conditions are needed. This makes the problem over-determined in most cases, so the initial conditions must be adjusted through iteration until the solutions obtained satisfy the original boundary conditions. As already mentioned, equation (1) is especially difficult to solve when ρ and its derivatives vanish faster than ϕ and E within regions of interest. But in those regions new initial conditions are easy to obtain, and therefore equation (2) can be solved without iterating. In that case the original boundary conditions are to be imposed only after a complete set of solutions is obtained.

The Langmuir-probe problem is a good example. Perturbations from the probe decay rapidly outside the sheath edge located at r_s and effectively vanish beyond the presheath radius, $r_{ps} \simeq 2r_s$. Modeling is therefore needed only within the sheath and presheath. Equally important, since the charge density decays rapidly past r_s, the potential ϕ_1 at an initial location $r_1 > r_s$ can be estimated by setting

$$\rho(r_1, \phi_1) = 0. \tag{6}$$

Newton's method or equivalent is sufficient for this purpose. Given ϕ_1, the field at r_1 can be estimated by setting the right-hand side of equation (2) to zero, thus producing the quasineutral result [23],

$$E_1 = E(r_1) = \frac{Q_c(r_1, \phi_1)}{k_s^2(r_1, \phi_1)}. \tag{7}$$

While expressions equivalent to (6) and (7) have been used previously, here they are applied well outside the sheath where the approximations are nearly exact. Since the solutions are advanced from r_1 to the probe surface r_o, the probe potential ϕ_o is now part of the solution rather than a boundary condition.

General expressions for k_s^2 and Q_c were given in [23] for plasmas in both fluid and kinetic forms, but in this work the fluid expressions simplify under the assumptions made by Allen *et al* [18]. In particular, the positive ions are taken to be cold and collisionless near the probe. The latter assumption is justified provided the ion mean free path greatly exceeds the presheath radius r_{ps}. In addition, particle creation and destruction are ignored near the probe. This assumption is usually well justified provided the unperturbed plasma is uniform out to a distance $r_w \gg r_{ps}$. Losses at the walls determine the total production rate in steady state, and therefore the average local production rate varies as the wall area divided by the plasma volume, or equivalently as r_w^{-1}. The perturbed volume around the probe is far smaller, so particle creation and destruction can usually be ignored in that region to order $r_{ps}/r_w \ll 1$.

In contrast to the positive ions, the flow velocities of the electrons and negative ions are small everywhere, so their densities ions obey the Boltzmann relationship,

$$n_k(r) = n_{ko}\mathrm{e}^{-eq_k\phi(r)/T_k}, \tag{8}$$

to a good approximation [17]. See, however, section 7. Here T_k is the temperature, eq_k is the charge and n_{ko} is the density of repelled species k in the unperturbed plasma.

4. Extended ABR model

Setting the potential to zero far from the probe, the flow velocities of the positive ions satisfy the energy-conservation relationship,

$$u_i(r) = \sqrt{-\frac{2eq_i\phi(r)}{m_i}}, \tag{9}$$

where m_i is the mass and $q_i e$ is the charge of positive-ion species i. All positive ions thus reach their individual sound speeds, $c_i = (q_i T_e/m_i)^{1/2}$, at the location where

$$e\phi(r_s) = -\frac{T_e}{2}. \tag{10}$$

The location r_s defines the outer edge of the sheath, and only within the sheath is the plasma highly charged. While the Bohm condition plays no formal role in the present calculations, it is met for this problem when $u_i = c_i$ for all positive ions. More generally (e.g. for a collisional presheath), the Bohm condition is met when some species are supersonic and others are subsonic [23, 24]. Note that the sheath formally exists (i.e. $r_s > r_o$) only when $e\phi_o < -T_e/2$.

In the absence of sources and sinks, the particle fluxes are conserved, and therefore the positive-ion densities satisfy

$$\begin{aligned}\frac{n_i(r)}{n_i(r_s)} &= \left(\frac{r_s}{r}\right)^\beta \frac{c_i}{u_i(r)} \\ &= \left(\frac{r_s}{r}\right)^\beta \sqrt{-\frac{T_e}{2e\phi(r)}},\end{aligned} \tag{11}$$

where $\beta = 0, 1, 2$ for planar, cylindrical and spherical probes, respectively. At large r the ion densities $n_i(r)$ approach the unperturbed values n_{io}, so $\phi(r)$ ultimately falls off as $r^{-2\beta}$ in equation (11). This is possible only for non-planar probes, $\beta > 0$, however. For planar probes, mechanisms other than geometrical curvature (e.g. ion collisions) determine the extent of the presheath [25]. Approximate solutions for planar probes can be obtained by making the probe radius r_o very large, but the results strictly apply only if all positive ions have the same mean free path.

Using equations (8) and (11), Poisson's equation can be written as

$$\begin{aligned}\frac{1}{r^\beta}\frac{d}{dr}r^\beta\frac{d\phi}{dr} &= -4\pi\rho_+(r_s)\left(\frac{r_s}{r}\right)^\beta\sqrt{-\frac{T_e}{2e\phi(r)}} \\ &\quad - 4\pi e\sum_k q_k n_{ko} e^{-eq_k\phi(r)/T_k}.\end{aligned} \tag{12}$$

Here the subscript i refers to positively charged species ($q_i > 0$), the subscript k refers to negatively charged species ($q_k < 0$) and $\rho_+(r_s)$ is the positive-charge density at the sheath edge. The boundary conditions are $\phi(r_o) = \phi_o$ and $\phi \to 0$ as $r \to \infty$.

To eliminate $\rho_+(r_s)$, consider the plasma current I_p flowing to the probe. Since the current carried by each species is independent of r in the absence of sources and sinks, the current carried by the positive ions satisfies

$$I_+ = I_+(r_s) = (2r_s)^\beta \pi e\sum_i q_i n_i(r_s) c_i. \tag{13}$$

Similarly, the flow velocities of the repelled species satisfy the kinetic condition, $u_k(r_o) = (T_k/2\pi m_k)^{1/2}$, at the probe, and therefore the negatively charged species carry a current given by

$$I_- = I_-(r_o) = (2r_o)^\beta \pi e\sum_k q_k n_{ko} e^{-eq_k\phi_o/T_k}\sqrt{\frac{T_k}{2\pi m_k}}. \tag{14}$$

Scaled to the electron-saturation current,

$$I_{es} \equiv -(2r_o)^\beta \pi e n_{eo}\sqrt{T_e/2\pi m_e}, \tag{15}$$

the total probe current is

$$\begin{aligned}i_p &\equiv \frac{I_p}{I_{es}} = \frac{I_+ + I_-}{I_{es}} \\ &= -\left(\frac{r_s}{r_o}\right)^\beta \sum_i q_i\left[\frac{n_i(r_s)}{n_{eo}}\right]\sqrt{\frac{2\pi q_i m_e}{m_i}} \\ &\quad - \sum_k q_k\alpha_k e^{-\Phi_o/\tau_k}\sqrt{\frac{|q_k\tau_k|\,m_e}{m_k}}.\end{aligned} \tag{16}$$

Here m_e is the electron mass, n_{eo} is the unperturbed electron density, $\Phi_o = -e\phi_o/T_e$, $\alpha_k = n_{ko}/n_{eo}$ and $\tau_k = -T_k/q_k T_e > 0$.

To utilize equation (16), observe that the positive-ion densities are all directly proportional to one another in equation (11), so

$$\frac{n_i(r_s)}{n_{ii}(r_s)} = \frac{\alpha_i}{\alpha_{ii}}, \tag{17}$$

where the subscripts i and ii refer to any positive-ion species. Equation (16) can thus be rearranged to produce

$$\begin{aligned}\frac{n_{ii}(r_s)}{\alpha_{ii}} &= -\left(\frac{r_o}{r_s}\right)^\beta n_{eo} \\ &\quad\times\left[\frac{i_p + \sum_k q_k\alpha_k e^{-\Phi_o/\tau_k}\sqrt{|q_k\tau_k|\,(m_e/m_k)}}{\sum_i q_i\alpha_i\sqrt{2\pi q_i m_e/m_i}}\right],\end{aligned} \tag{18}$$

and therefore

$$\begin{aligned}\rho_+(r_s) &= e\sum_i q_i n_i(r_s) = \frac{e n_{ii}(r_s)}{\alpha_{ii}}\sum_i q_i\alpha_i \\ &= \gamma\sqrt{2}e n_{eo}(r_o/r_s)^\beta.\end{aligned} \tag{19}$$

Here

$$\begin{aligned}\gamma &\equiv -\frac{\sum_i q_i\alpha_i}{\sum_i q_i\alpha_i\sqrt{4\pi q_i m_e/m_i}} \\ &\quad\times\left[i_p + \sum_k q_k\alpha_k e^{q_k\Phi_o/\tau_k}\sqrt{|\tau_k q_k|\,(m_e/m_k)}\right].\end{aligned} \tag{20}$$

Given equation (19), Poisson's equation (12) can be written in dimensionless units as

$$\frac{1}{\chi^\beta}\frac{d}{d\chi}\chi^\beta\frac{d\Phi}{d\chi} = \left(\frac{\chi_o}{\chi}\right)^\beta\frac{\gamma}{\sqrt{\Phi}} + \sum_k q_k\alpha_k e^{-\Phi/\tau_k}, \tag{21}$$

where $\Phi = -e\phi/T_e$, $\chi = r/\lambda_{De}$, $\chi_o = r_o/\lambda_{De}$ and $\lambda_{De} = (T_e/4\pi e^2 n_{eo})^{1/2}$ is the electron Debye length. Equation (21),

which is structurally similar to that given by Kennedy and Allen [26], has physical solutions only when γ lies between 0 and $\gamma_{\max}$, where $\gamma_{\max}$ depends on the dimensionless probe radius χ_o. To change the dimensionless probe voltage $\Phi_o = \Phi(\chi_o)$, change γ. By this means the function $\gamma(\Phi_o)$ can be calculated. Once $\gamma(\Phi_o)$ is known, compute the dimensionless probe current using

$$i_p(\Phi_o) = -\sum_k q_k \alpha_k e^{-\Phi_o/\tau_k} \sqrt{\frac{|q_k \tau_k| m_e}{m_k}} - \gamma(\Phi_o) \frac{\sum_i q_i \alpha_i \sqrt{4\pi q_i m_e / m_i}}{\sum_i q_i \alpha_i}. \quad (22)$$

For Maxwellian electrons in electropositive plasmas, equation (22) reduces to

$$i_p(\Phi_o) = e^{-\Phi_o} - \gamma(\Phi_o) \sum_i q_i \alpha_i \sqrt{4\pi q_i m_e / m_i}, \quad (23)$$

based on the charge-neutrality condition, $\Sigma q_i \alpha_i + \Sigma q_k \alpha_k = 0$.

Equations (21) and (22) constitute the extended ABR model, and from these equations several conclusions can be drawn. First, the particle masses appear in equation (22) but not (21). The same is true for the number of positive-ion species and the density factors α_i. Accordingly, neither the particle masses nor the number and nature of the positive-ion species has any direct effect on the potential $\phi(r)$ outside the probe! The dimensionless probe potential Φ_o can therefore be computed in electropositive plasmas as a function of γ without knowing the ion composition. Moreover, given the ion composition and $\gamma(\Phi_o)$, the probe characteristic $i_p(\Phi_o)$ can be obtained using equation (23). Since equations (22) and (23) are purely algebraic, the major positive-ion constituents can be identified, in principle, through careful curve-fitting of experimental data for $I_p(\phi_o)$.

A similar conclusion applies to electronegative plasmas, provided the negative ions are all singly charged and have the same temperature. In that case Poisson's equation reduces to $\nabla^2\Phi = \gamma(\chi_o/\chi)^\beta \Phi^{-1/2} - e^{-\Phi} - \alpha_o e^{-\Phi/\tau}$, where $\alpha_o = \sum_{k\neq e} \alpha_k$ is the electronegativity in the unperturbed plasma. Hence, once α_o and the negative-ion temperature τ are specified, $\gamma(\Phi_o)$ can be determined as before, and careful curve-fitting of $I_p(\phi_o)$ can again help reveal the ion composition. Electrons with two or more temperatures are equally easy to treat, after specifying the temperature and fractional density of each electron component.

5. New field equation

Although simple in form, equation (21) is difficult to solve, especially far from the probe. Fortunately, these difficulties can be overcome by taking the derivative of equation (21) and solving the new equation as an initial-value problem. The new equations are

$$\frac{d}{d\chi}\left[\frac{1}{\chi^\beta}\frac{d(\chi^\beta \varepsilon)}{d\chi}\right] = k^2\varepsilon - Q, \quad (24)$$

where

$$\frac{d\Phi}{d\chi} = -\varepsilon, \quad (25)$$

$$k^2 = -\frac{\gamma}{2\Phi^{3/2}}\left(\frac{\chi_o}{\chi}\right)^\beta - \sum_k \left(\frac{q_k \alpha_k}{\tau_k}\right) e^{-\Phi/\tau_k} \quad (26)$$

and

$$Q = -\frac{\beta\gamma\chi_o^\beta}{\chi^{\beta+1}\sqrt{\Phi}}. \quad (27)$$

To determine the initial conditions, first specify values for γ, the dimensionless probe radius $\chi_o = r_o/\lambda_{De}$, the curvature factor β (1 for cylinders, 2 for spheres), and the relative fraction α_k, charge q_k and temperature τ_k of each negatively charged species. Then choose a starting location χ_1 outside the sheath such that $\Phi(\chi_1) \equiv \Phi_1 < 0.5$. For example, if the sheath is as wide as $10\lambda_{De}$, choose $\chi_1 \geqslant \chi_o + 15$. To model the entire presheath, make $\chi_1 > 2\chi_o$. The potential Φ_1 is obtained by setting the right-hand side of equation (21) to zero, which yields the transcendental equation,

$$\sqrt{\Phi_1}\sum_k q_k \alpha_k e^{-\Phi_1/\tau_k} = -\gamma\left(\frac{\chi_o}{\chi_1}\right)^\beta. \quad (28)$$

This equation can be solved using Newton's method or equivalent. Similarly, to determine the field at χ_1, set the right-hand side of equation (24) to zero, to obtain

$$\varepsilon(\chi_1) = \frac{Q(\chi_1, \Phi_1)}{k^2(\chi_1, \Phi_1)}. \quad (29)$$

Use the same procedure to determine starting values at the next location, $\chi_2 = \chi_1 - \Delta\chi$ as needed. Recall that approximations (28) and (29) become nearly exact a short distance beyond the sheath edge χ_s.

The complete model consists of equations (24)–(27), the initial conditions (28) and (29), and equation (22) for the probe current. To maintain stability, advance ε implicitly by evaluating $k^2\varepsilon$ at the new location and Q at the old location in equation (24); see appendix A. Use equation (25) twice per step, the first time to determine k^2 at the new location and the second time to advance Φ using an average value for ε. For accuracy, restrict the step size to $\Delta\chi \leqslant 0.05$; highly electronegative plasmas require even smaller steps. Advance the solutions up to the probe surface, $\chi = \chi_o$. To change the probe bias Φ_o while avoiding unphysical solutions, start with γ small but positive and then raise it slowly.

The parameters k^2 and Q in equations (25) and (26) were obtained by taking the derivative of equation (21), but they could have been derived by applying the assumptions made earlier to the fluid expressions given in [23]. In particular, the general fluid expression for the screening factor in dimensional form is

$$k_s^2 = 4\pi e^2 \sum_j \frac{q_j^2 n_j}{T_j - m_j u_j^2}, \quad (30)$$

where the sum extends over all species. As discussed in [23], k_s^2 varies widely within the plasma. Far from the probe, the fluid velocities $u_j \to 0$ so $k_s^2 \to \lambda_D^{-2} \equiv 4\pi e^2 \Sigma q_j^2 n_j / T_j$. Unlike

the electron Debye length λ_{De}, the plasma Debye length λ_D depends on the temperatures and densities of *all* the species, and if one or more of these species is cold, $\lambda_D \to 0$ and $k_s^2 \to +\infty$. Extremely small spatial steps are therefore needed to solve Poisson's equation directly far from the probe; as noted in [23], this region can be modeled more efficiently by assuming quasineutrality. Closer to the probe, k_s^2 diverges again and becomes discontinuous whenever $m_j u_j^2 = T_j$. However, these discontinuities do not appear in the ABR model, because $m_k u_k^2$ remains less than T_k for the negative species while $T_i = 0$ for the positive species. Therefore k_s^2 only becomes more negative outside the sheath. Within the sheath the positive-ion velocities u_i become so large that $|k_s^2|$ becomes comparable to λ_{De}^{-2}. Hence, the electron Debye length λ_{De}, not the plasma Debye length λ_D, largely governs electrostatic shielding around the probe. By using equation (24) in place of Poisson's equation, all regions in the ABR model can be modeled stably using spatial steps larger than λ_D but smaller than λ_{De}. See appendix A for further discussion.

Because Poisson's equation (21) is never formally invoked, it can be used as a diagnostic. The diagnostic is useful, however, only in regions where $\varepsilon \geqslant \Delta\chi$, because ε is known only to that order. Fortunately, approximation (29) is well justified when ε is small, so the solutions should satisfy either equation (21) or (29) for all χ. For the solutions presented next, one or both conditions were satisfied to 5% or better.

6. Examples

For the first example, consider a spherical probe with a normalized radius $\chi_o = 10$ and a bias $\Phi_o = 30$ in an electropositive plasma. Because the bias is large, the positive-charge density first decreases outside the probe and then increases, as shown in figure 1(*a*). Geometrical curvature accounts for the decrease. In contrast, the electron density rises monotonically from near zero at the probe, while the potential $\Phi(\chi)$ in figure 1(*b*) falls.

Figure 2 plots $\gamma(\Phi_o)$ for three values of χ_o, and from plots like this, equation (23) can be used to compute the normalized probe current $i_p(\Phi_o)$ in any electropositive plasma. Figure 3(*a*) shows $i_p(\Phi_o)$ for argon ions and two different-sized spherical probes, and figure 3(*b*) shows a blowup in ion saturation. As the bias is raised, the sheath widens, so the sheath radius r_s and incoming ion current grow. The ion current grows significantly, however, only if the sheath width is comparable to or larger than the probe radius r_o. This was true for the small probe but not the large probe. As expected, the values obtained for $i_p(\Phi_o)$ agree almost exactly with the ABR results listed by Laframboise [10].

To correlate better with experiment, the potentials in figure 3 were shifted by $\Phi_w = 5.17$, which is the floating potential computed for a very large probe ($\chi_o = 10^4$). This shift crudely compensates for the sheath drop occurring at the grounded walls. The code prediction agrees with the value given by planar theory, $\Phi_w = 0.5[1 + \ln(m_i/2\pi m_e)]$, to within 0.1%. More generally, the floating potential at distant walls

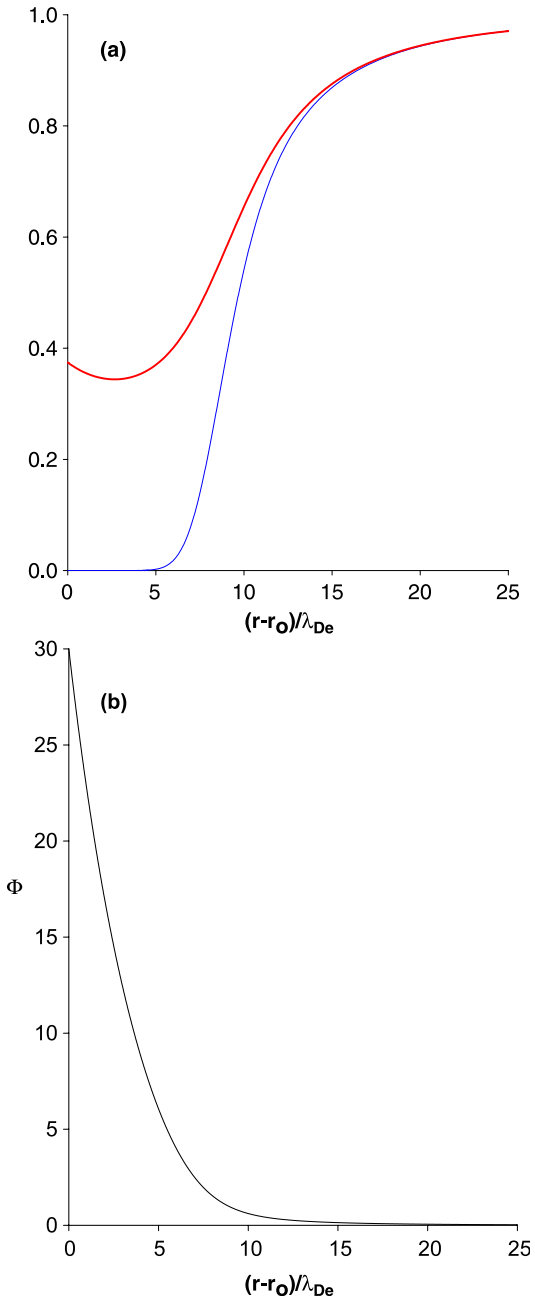

Figure 1. Spherical probe with normalized radius $\chi_o = 10$ and bias $\Phi_o = 30$ in an electropositive plasma. (*a*) Normalized electron density n_e/n_{eo} (thin, lower curve) and positive-charge density ρ_+/en_{eo} (thick, upper curve) versus normalized distance from the probe. (*b*) Normalized potential $\Phi(\chi)$.

($\chi_o \to \infty$) satisfies

$$\frac{\sum_k q_k \alpha_k e^{-\Phi_w/\tau_k}\sqrt{|q_k|\,\tau_k/m_k}}{\sum_k q_k \alpha_k e^{-0.5/\tau_k}} = \frac{\sum_i q_i \alpha_i \sqrt{2\pi/m_i}}{\sum_i q_i \alpha_i}, \qquad (31)$$

which can be obtained by assuming quasineutrality at $r_s \to \infty$.

Shown in figure 3(*c*) is the current for the small probe in a 50/50 mix of argon and helium ions. The ion current is significantly larger while the wall potential Φ_w is slightly less. In this case, Φ_w agreed with equation (31) to within 2%; reducing the step size $\Delta\chi$ improves the agreement. For the runs presented here, $\Delta\chi$ ranged from 0.004 to 0.06.

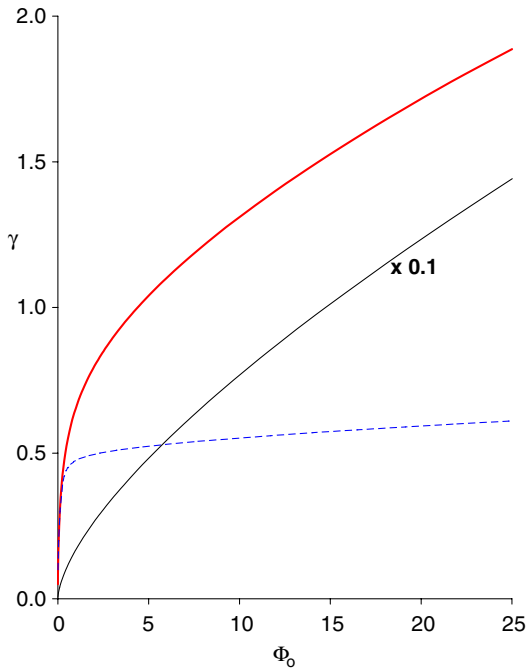

Figure 2. Scaling parameter γ versus bias Φ_o for a spherical probe for χ_o equal to 1 (thin, lower curve, multiplied by 0.1), 10 (thick, upper curve) and 100 (dashed curve).

A comparison of spherical and cylindrical probes is shown in figure 4, again for $\chi_o = 10$. The wall potential Φ_w was the same in both cases, and the two curves overlap when Φ_o is small but not when Φ_o is large; see figure 4(*b*). As Φ_o is raised, the sheath radius r_s increases faster for the cylinder than for the sphere, but because the sheath area varies as r_s^2 for the sphere and as r_s for the cylinder, the ion current rises faster for the sphere.

General solutions for $\Phi(\chi)$ and $\gamma(\Phi_o)$ can be obtained in electronegative plasmas as well, provided the negative ions are all singly charged and have the same normalized temperature τ. In that case $\gamma(\Phi_o)$ depends only on τ, χ_o and the total electronegativity α_t. For example, figure 5(*a*) shows a plot of $\gamma(\Phi_o)$ for a spherical probe with $\chi_o = 10$ in a plasma with $\alpha_t = 49$ and $\tau = 0.1$. Figure 5(*b*) plots the normalized electron density n_e/n_{eo}, the positive-charge density ρ_+/en_{eo}, and the local electronegativity, $\alpha_l(\chi) = \sum_{k\neq e} n_k(\chi)/n_{eo}$ The probe bias is $\Phi_o = 5$. As before, the probe current $i_p(\Phi_o)$ depends on the makeup of the plasma, and in this case equation (22) reduces to

$$i_p = e^{-\Phi_o/\tau} \sum_k \alpha_k \sqrt{\tau m_e/m_k} - \frac{\gamma(\Phi_o)}{1+\alpha_t} \sum_i q_i \alpha_i \sqrt{4\pi m_e/m_i}. \tag{32}$$

A sample plot for Cl_2 is shown in figure 5(*c*), with the positive ions consisting of 90% Cl^+ and 10% Cl_2^+ and the negative ions consisting of 90% Cl^- and 10% Cl_2^-. For convenience, the current in figure 5(*c*) was normalized to the sum of the electron and negative-ion currents at $\Phi_o = 0$ rather than to the electron current alone. Compared with the electropositive plasma in figure 3, the normalized probe current is much larger in magnitude at $\Phi_o > \Phi_w$, and $\Phi_w = 2.38$ is smaller.

Results for two-temperature electrons in argon are presented in figure 6. Most of the electrons had a temperature $\tau = 1$ as before, but 2% had $\tau = 9$. The small, hot component raised the floating potential Φ_w from 5.17 to 21.0, assuming the hot component persists to the walls. However, to better compare with single-temperature electrons, the current in figure 6 was normalized to the total electron current at $\Phi_o = 0$, and the potential was not shifted. As is evident, the hot component had only a weak effect near electron saturation in figure 6(*a*) but a strong effect near ion saturation in figure 6(*b*).

7. Discussion

Several experimental difficulties have long plagued Langmuir probes, and one problem is that the values obtained for the bulk plasma density n_o in ion saturation ($\Phi_o > \Phi_w$) do not always agree with those obtained in electron saturation ($\Phi_o < \Phi_w$) [1–8]. At first glance, ion saturation appears to be the better choice [5, 8], because the plasma and probe are less perturbed and because the positive-ion current is insensitive to the probe voltage. In particular, if the probe is very large, the positive-ion current I_+ saturates at a level proportional to n_o times the surface area of the probe times the mean ion sound speed. Since the latter two parameters are well known or can be estimated, the plasma density n_o can be easily determined from I_+.

However, the probe current I_p approaches I_+ only if the high-energy tail of the electron energy distribution is not over-populated. Electron–electron collisions keep the distribution close to Maxwellian at low energy but become ineffectual at high energy. While a small over-population has little effect in electron saturation, it can have a large effect in ion saturation, as shown in figure 6(*b*). Over-simplified models of ion saturation can therefore significantly underestimate n_o, depending on the electron energy distribution.

In electropositive plasmas, $I_p(\phi_o)$ is largely determined by electrons alone when $\Phi_o \leqslant 3$, and therefore n_o can often be determined more accurately using electron saturation rather than ion saturation [1, 4]. The present analysis applies only up to the plasma potential, which to a good approximation is the voltage where $dI_p/d\phi_o$ is a maximum [4]. At the plasma potential (taken as $\Phi = 0$ in this work), the probe current I_p is approximately equal to the probe area times $en_o\sqrt{T_e/2\pi m_e}$. The electron temperature T_e can be determined from $d\ln I_e/d\phi_o$, where the electron current I_e equals I_p minus the total ion current. The ion current is usually extrapolated from ion saturation using a power-law fit, but the physical basis for such a fit is weak [4, 14]. Better estimates can be obtained using the present model.

The full probe characteristic $I_p(\phi_o)$ provides more information than single portions alone, and even a cursory examination is useful. For example, an over-populated electron tail is indicated if I_p turns negative more slowly than expected as Φ_o is raised, while an under-populated tail is indicated if I_p turns negative faster than expected. And an electronegative plasma is indicated if I_p is unusually large and negative when $\Phi_o > 7$. In principle, the positive-ion current I_+

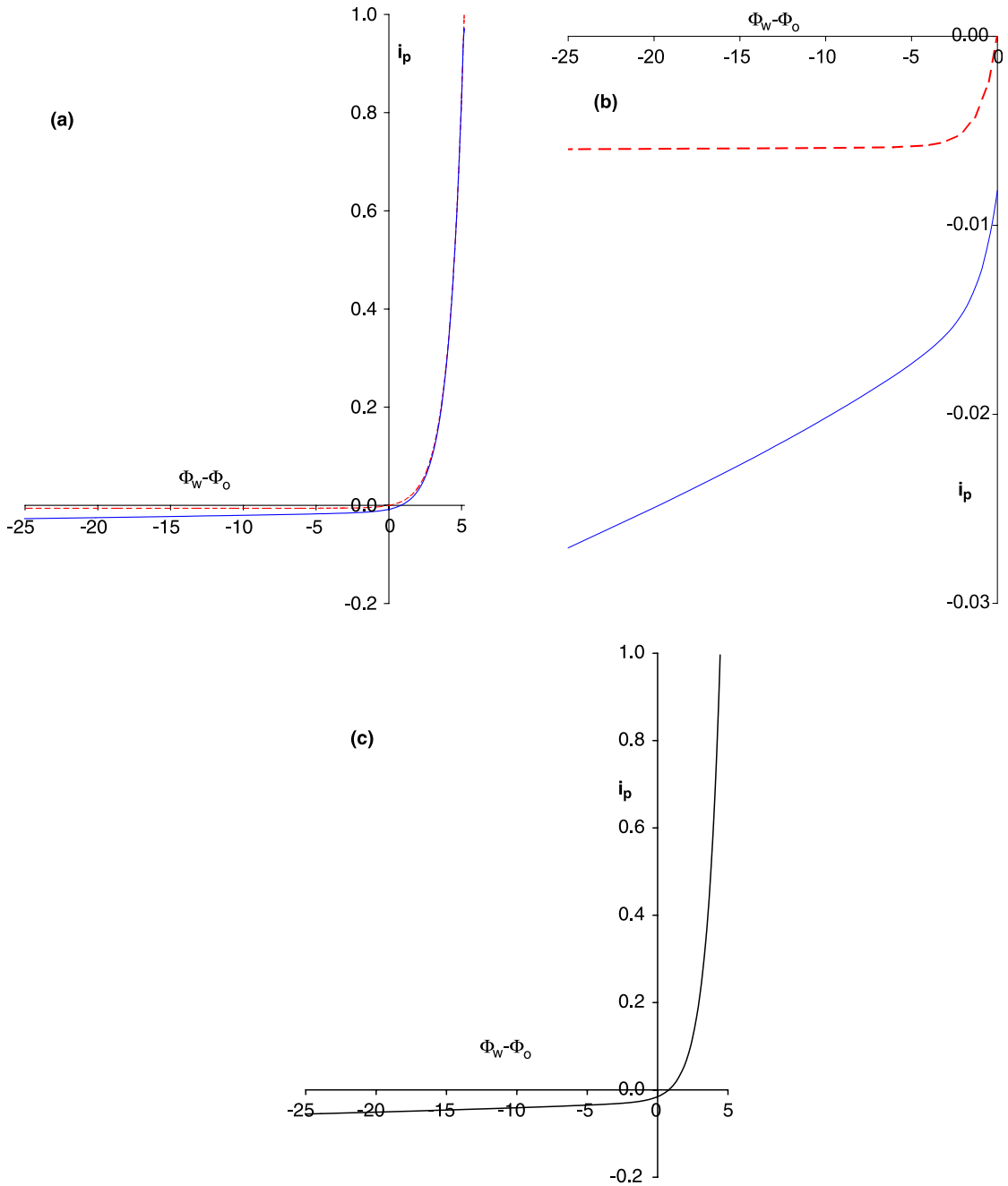

Figure 3. (*a*) Normalized current $i_p(\Phi_o)$ in argon for a spherical probe with χ_o equal to 10 (solid curve) and 10^3 (dashed curve). (*b*) Expanded scale in ion saturation. (*c*) Probe current $i_p(\Phi_o)$ for a 50/50 mix of argon and helium ions for $\chi_o = 10$. The wall potential Φ_w, which is the floating potential at $\chi_o = 10^4$, was 5.17 in pure argon and 4.45 in the mixture.

can be used to help identify the major positive-ion constituents, while the slope $dI_+/d\phi_o$ can be used to help confirm estimates of the electron Debye length λ_{De}. Similarly, the negative-ion current can be used to verify the temperature and composition of the negative ions, while the electron current $I_e(\phi_o)$ gives the electron energy distribution [4]. However, extracting the individual currents from I_p is exceedingly difficult, and therefore the present model is mainly useful for confirming assumptions already made.

A second controversy concerns the relative merits of spherical and cylindrical probes [5, 8, 10–15]. Cylindrical probes are more widely used, because they are simple to construct and because the shaft supporting the probe can be aligned with the probe axis [11]. In addition, cylindrical probes can be reoriented, which is useful if the plasma is flowing or if an external magnetic field or ionizing beam is present. However, the potential $\phi(r)$ falls off more slowly outside a cylindrical probe than a spherical probe of the same radius, so more of the plasma is perturbed. Cylindrical probes also trap more positive ions in closed orbits around the probe [12], and cylindrical probes must be long to neglect end effects [2] but not so long as to compromise spatial resolution. The latter problem can potentially be overcome by using a very long probe but with current collected only from one or more short

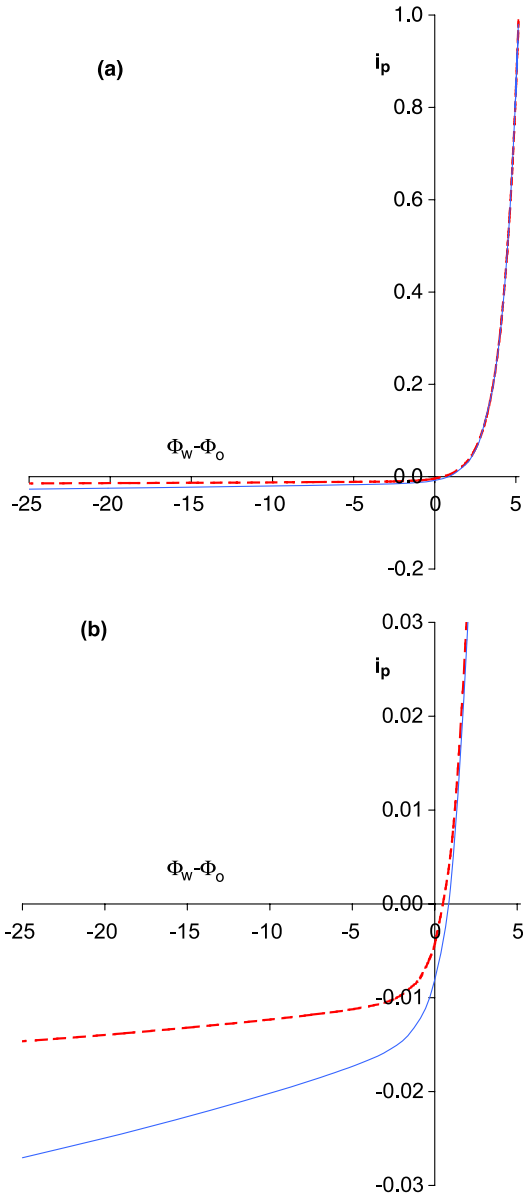

Figure 4. (a) Probe characteristic $i_p(\Phi_o)$ in argon for a spherical probe (solid curve) and a cylindrical probe (dashed curve) with $\chi_o = 10$. (b) Expanded scale in ion saturation.

segments. In all cases the surface area of the probe should be large to produce detectable signals.

A related theoretical controversy is the cold-ion paradox [10, 26]. The temperature T_i of the positive ions is zero in ABR theory but nonzero in BR theory. Although the two theories should converge as $T_i \to 0$, they do so only for spherical probes. Indeed, even the radial dependence of $\phi(r)$ differs between the two theories for cylindrical probes [10]. Moreover, while BR theory would appear to be superior [3, 10], ABR theory often agrees better with experiment [1, 6, 13]. A partial explanation for this behavior was provided by Stangeby and Allen [27].

Both theories neglect ionization and assume collisionless ions and an unbounded plasma. Ion angular momentum and energy are then both conserved, so ions just grazing the probe have an angular momentum satisfying $J_{gi} = m_i r_o u_i(r_o) = r_o\sqrt{2m_i(E_i - eq_i\phi_o)}$. Here u_i is the ion speed and E_i is the initial ion energy. BR theory uses this relationship to identify which positive ions strike the probe and which do not, but both theories apply only out to a radius r_{max} where collisions, ionization, or plasma size becomes important. BR theory applies only if $J_{max} \equiv r_{max}\sqrt{2m_i E_i} > J_{gi}$ for every positive ion species i; otherwise all ions of species i lying within r_{max} are collected, as assumed in ABR theory. ABR theory, on the other hand, assumes cold positive ions and zero angular momentum and thus applies only if $E_i \ll |eq_i\phi_o|$ and $J_{max} \ll J_{gi}$. Since neither model strictly applies when J_{max} is smaller than but comparable to J_{gi}, the two theories need not converge as $E_i \to 0$.

The presheath radius r_{ps} marks the beginning of the unperturbed plasma, and therefore the ABR model generally applies as long as the initial ion temperature satisfies

$$T_i \ll \left(\frac{r_o}{r_{ps}}\right)^2 |eq_i\phi_o| \tag{33}$$

for all positive ions. Since r_{ps} is approximately equal to twice the sheath radius r_s, condition (33) is usually met provided $r_o \geqslant \lambda_{De}$ and $e\phi_o \leqslant -20T_i$. Otherwise the BR model should be used.

Unlike positive ions, the electrons and negative ions cannot be treated as cold, because these species reach the probe only if their initial energy satisfies $E_k \geqslant eq_k\phi_o$. These species are commonly treated using the Boltzmann relationship (8), and this relationship is justified as long as the first and last terms in the momentum equation,

$$\frac{d}{dr}\left(\frac{m_k u_k^2}{2}\right) + T_k\frac{d\ln(n_k)}{dr} = eq_k E - \nu_k m_k u_k, \tag{34}$$

are negligible. The last term is negligible at low gas pressure because the collision frequency ν_k is small. The inertial term is small as well, because $m_k u_k^2/2 \leqslant T_k/4\pi \ll T_k$, based on the kinetic condition at the probe. However, the inertial term is truly negligible only if the probe bias is sufficiently large. To show this, combine flux conservation with the kinetic condition to obtain

$$u_k(r) = \frac{n_k(r_o)}{n_k(r)}\left(\frac{r_o}{r}\right)^\beta\sqrt{\frac{T_k}{2\pi m_k}}. \tag{35}$$

This expression together with the Boltzmann relationship (8) for $n_k(r)$ indicates that

$$\frac{d}{dr}\left(\frac{m_k u_k^2}{2}\right) = \frac{e^{2eq_k[\phi_o-\phi(r)]/T_k}}{2\pi}\left(\frac{r_o}{r}\right)^{2\beta}\left[eq_k E(r) - \frac{\beta T_k}{r}\right]. \tag{36}$$

The first term in equation (34) is therefore negligible at the probe (and everywhere else) for all repelled species k only if

$$|eE(r_o)r_o| \gg \beta T_e/2\pi, \tag{37}$$

assuming electrons are the hottest species. The field $E(r_o)$ typically varies as the probe voltage ϕ_o divided by the electron Debye length λ_{De}, and thus the Boltzmann relationship is generally justified only if

$$\Phi_o\chi_o > 1. \tag{38}$$

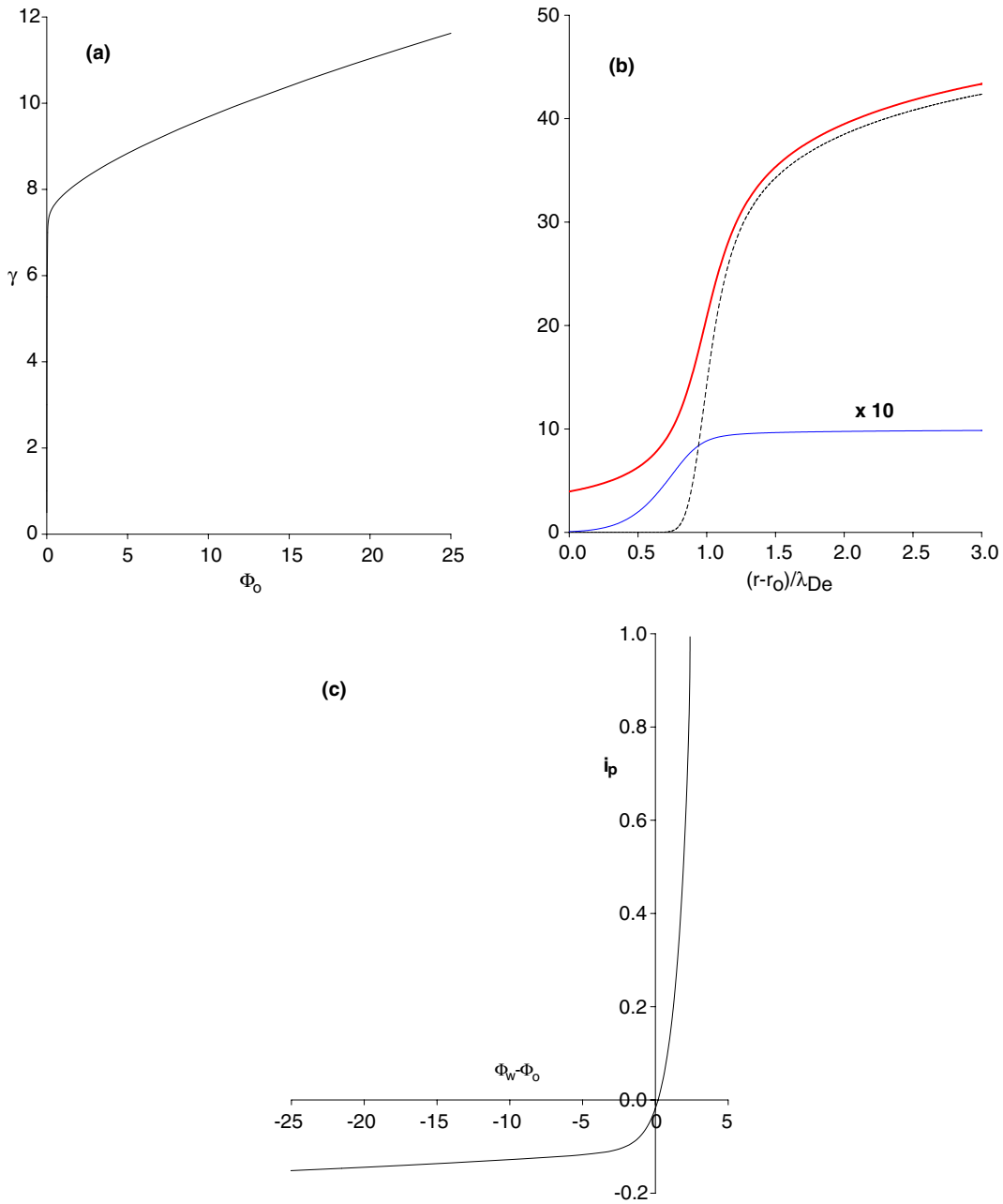

Figure 5. Electronegative plasma with electronegativity $\alpha_t = 49$ and normalized negative-ion temperature $\tau = 0.1$ for a spherical probe and $\chi_o = 10$. (*a*) $\gamma(\Phi_o)$. (*b*) Normalized electron density n_e/n_{eo} (thin curve, multiplied by 10), local electronegativity α_l (dashed curve) and positive-charge density ρ_+/en_{eo} (thick uppermost curve) for $\Phi_o = 5$. (*c*) Probe characteristic $i_p(\Phi_o)$ in Cl_2 (see text), renormalized to the total negative current at $\Phi = 0$. Wall potential $\Phi_w = 2.38$.

This restriction applies to any model using the Boltzmann relationship, and hence these models work best for large probes. Note that even if the Boltzmann relationship is justified near the probe, it may not be justified far from the probe if the plasma is highly electronegative or collisional [23].

The final controversy is whether analytical solutions obtained in the sheath can be joined smoothly to those in the presheath, since different scale lengths govern the two regions [28–30]. Lam [31] and Riemann [28] used fluid theory to study the transition in plasmas containing Maxwellian electrons and one ion species, but their conclusions apply for any plasma governed by two distinct scale lengths. Spherical and cylindrical probes satisfy this requirement provided: (i) the plasma is electropositive; (ii) the electrons are Maxwellian; (iii) the ions are collisionless and (iv) sources and sinks are negligible throughout the sheath and presheath. In that case the electron Debye length λ_{De} and the sheath radius r_s fully characterize the problem.

The sheath edge χ_s is the location where quasineutrality first applies, and making that assumption, Poisson's equation reduces to $\nabla^2\Phi = (\chi_s/\chi)^\beta e^{-\Phi_s}\sqrt{\Phi_s/\Phi} - e^{-\Phi}$, where $\Phi_s = \Phi(\chi_s)$. Quasineutrality fails catastrophically when $\Phi = 0.5$,

so this value is commonly used for Φ_s. However, other definitions are equally valid and often work better. To model the region near χ_s, rewrite Poisson's equation in terms of the variables,

$$\xi = \left(\frac{\chi}{\chi_s} - 1\right)\chi_s^{h_1}, \qquad \eta = (\Phi - \Phi_s)\chi_s^{h_2}. \tag{39}$$

The coefficients h_1 and h_2 can then be determined by expanding Poisson's equation to lowest order in ξ and η about χ_s. This leads to

$$\chi_s^{2h_1-h_2-2}\frac{d^2\eta}{d\xi^2} = (\chi_s^{-2h_2}\eta^2 - \beta\chi_s^{-h_1}\xi)e^{-\Phi_s}, \tag{40}$$

where η was kept to second order on the right-hand side because the first-order terms cancel. The dependence on χ_s vanishes provided

$$2h_1 - h_2 - 2 = -2h_2 = -h_1, \tag{41}$$

and therefore $h_1 = 4/5$ and $h_2 = 2/5$. The electric field at the sheath edge thus obeys [28]

$$\begin{aligned} eE(r_s) &= -e\left.\frac{d\phi}{dr}\right|_{r=r_s} \\ &= \left(\frac{T_e}{\lambda_{De}}\right)\left.\frac{d\Phi}{d\chi}\right|_{\chi_s} = \left(\frac{T_e}{\lambda_{De}}\right)\chi_s^{h_1-h_2-1}\left.\frac{d\eta}{d\xi}\right|_{\xi=0} \\ &= \frac{T_e}{\lambda_{De}^{2/5}r_s^{3/5}}\left.\frac{d\eta}{d\xi}\right|_{\xi=0} \sim -\frac{T_e}{\lambda_{De}^{2/5}r_s^{3/5}}, \end{aligned} \tag{42}$$

where $d\eta/d\xi \sim -1$ at $\xi = 0$ by assumption.

The present code results support these claims. For example, choosing $\Phi_s = 0.5$ and $\Phi_o = 25$, the field in the code varied as $eE(r_s)/T_e \simeq -1.14\lambda_{De}^{-0.415}r_s^{-0.585}$ at the sheath edge to within a few per cent for $1 \leqslant r_o/\lambda_{De} \leqslant 10^4$. This result agrees well with equation (42), especially considering that the plasma is not truly quasineutral at $\Phi = 0.5$. While equation (40) is valid only over a narrow spatial range [29], the probe radius r_o nevertheless affects the sheath width, $\Delta\chi_s \equiv \chi_s - \chi_o$. For example, in the aforementioned problem the sheath width grew as $\Delta\chi_s \simeq 3.3 + 3\ln(\chi_o)$, and it thus increased by nearly an order of magnitude as χ_o rose from 1 to 10^4.

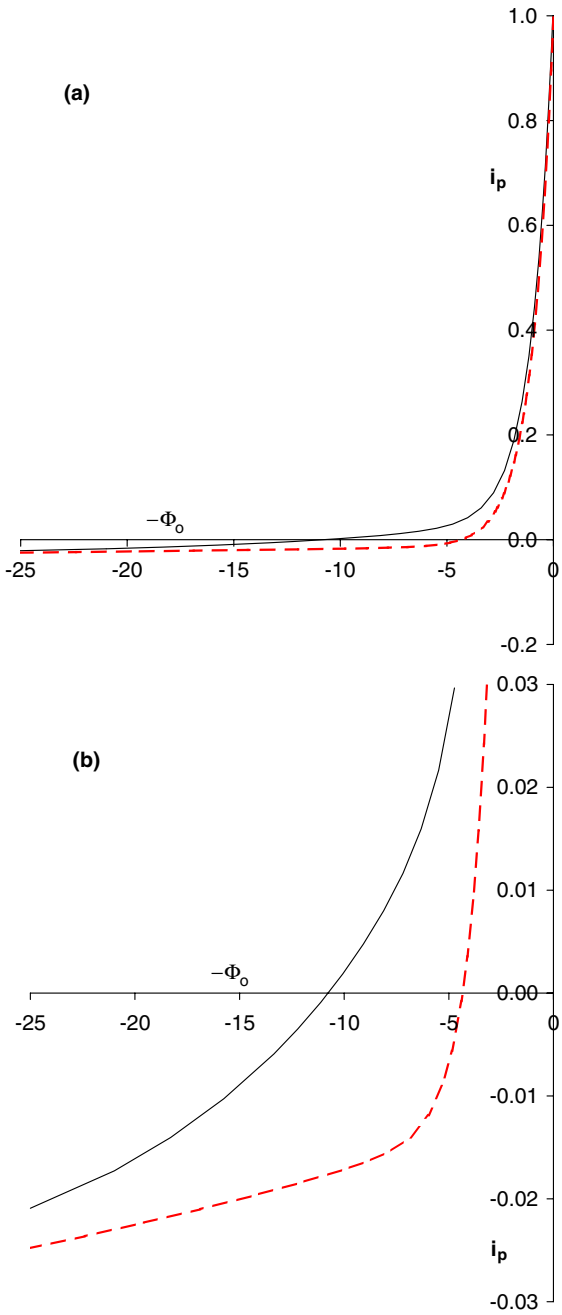

Figure 6. Spherical probe with $\chi_o = 10$ in argon. Solid curve: 98% of the electrons have a temperature $\tau = 1$ while the remainder (2%) have $\tau = 9$. Dashed curve: $\tau = 1$ for all electrons. (*a*) Probe characteristic $i_p(\Phi_o)$. (*b*) Expanded scale in ion saturation.

8. Conclusion

Langmuir-probe data are commonly interpreted using highly simplified models, most of which are valid only in plasmas containing Maxwellian electrons and a single ion species. While existing theories can easily accommodate more than two plasma species, direct numerical solution of Poisson's equation remains difficult. In this work a numerical scheme based on solving the derivative of Poisson's equation was presented. The new equation is linear in the electric field and can thus be solved implicitly and stably. Accordingly, the probe characteristic $I_p(\phi_o)$ can be computed quickly and easily for spherical or cylindrical probes in a wide range of plasmas. Results were presented using the radial-motion theory developed by Allen *et al* [18] for cold ions, but the numerical scheme should work equally well with the orbital-motion theory proposed by Bernstein and Rabinowitz [19] for warm ions. Both models are easy to code, and once coded, the models should enable researchers to make better use of experimental data. Sample solutions were given for multi-component electropositive plasmas, electronegative plasmas, and plasmas containing two-temperature electrons.

Acknowledgments

I am indebted to Professor Mikhail Benilov for pointing out the advantages of equation (24), which had been derived earlier [23] but not fully appreciated. I also thank Drs David Walker, Steven Slinker, and Paul Bernhardt for attempting to solve (unsuccessfully) Poisson's equation using commercial software and software developed in-house. This work was supported by the Office of Naval Research.

Appendix A. Numerical stability

Setting the curvature factor β to zero for convenience, equation (24) reduces to $\mathrm{d}^2\varepsilon/\mathrm{d}\chi^2 = k^2\varepsilon - Q$. This equation can be solved implicitly using

$$\varepsilon_{n+1} = \frac{2\varepsilon_n - \varepsilon_{n-1} - \Delta\chi^2 Q_n}{1 - \Delta\chi^2 k_{n+1}^2}, \tag{A1}$$

where $\varepsilon_n = \varepsilon(\chi_n)$, $Q_n = Q(\chi_n, \Phi_n)$, $k_n^2 = k^2(\chi_n, \Phi_n)$, and $\Phi_n = \Phi(\chi_n)$. Because the solutions are advanced inward, set $\chi_{n+1} = \chi_n - \Delta\chi$, where the step size $\Delta\chi > 0$. To determine k_{n+1}^2, set

$$\Phi_{n+1} = \Phi_n + \Delta\chi \cdot \varepsilon_n \tag{A2}$$

as a first approximation. After computing ε_{n+1}, reset the potential to

$$\Phi_{n+1} = \Phi_n + \Delta\chi \left(\frac{\varepsilon_{n+1} + \varepsilon_n}{2}\right). \tag{A3}$$

The stability properties of (A1) can be assessed by treating k^2 and Q as constant and considering solutions of the form $\tilde{\varepsilon}_n = \varepsilon_n + \delta e^{i\nu n}$. Here ε_n is the true numerical solution, $\delta\mathrm{e}^{i\nu n}$ is the error, and ν is in general complex. Applied to (A1), one finds that

$$\nu_i \equiv \mathrm{Im}(\nu) = 0.5\ln(1 - k^2\Delta\chi^2). \tag{A4}$$

In the ABR model $k^2 < 0$ outside the sheath, so in this region the solutions are stable, $\nu_i \geqslant 0$, for all $\Delta\chi$. Moreover, the solutions properly converge to $\varepsilon \to Q/k^2$ when $\Delta\chi \gg |k^2|^{-1/2}$. Inside the sheath, however, k^2 is sometimes positive, and the solutions are then stable only if $\Delta\chi < k^{-1}$. In electropositive plasmas, $|k| \sim 1$ inside the sheath, so limit the step size to $\Delta\chi < 1$. For accuracy, set $\Delta\chi \leqslant 0.05$. In highly electronegative plasmas k^2 can exceed unity, so even smaller steps are needed.

Appendix B. Linearization

Any analytic function or differential equation can be transformed into a linear expression through differentiation, and to show this, consider the general equation,

$$g(y_n, y_{n-1}, ..., y, x) = 0, \tag{B1}$$

where $y_n \equiv \mathrm{d}^n y/\mathrm{d}x^n$ and $y_o \equiv y$. Assume for convenience that $y_n, \ldots, y$ are known or can be determined at some position x_1. If g is nonlinear in either y_n or y_{n-1}, differentiate (B1) to obtain $\mathrm{d}g/\mathrm{d}x = 0 = (\partial g/\partial x) + \Sigma(\partial g/\partial y_s)y_{s+1}$, where the sum over s extends from 0 to n. Rearrangement produces

$$\frac{\mathrm{d}y_n}{\mathrm{d}x} = -\left(\frac{\partial g}{\partial y_n}\right)^{-1}\left(\frac{\partial g}{\partial x} + \sum_{s=0}^{n-1}\frac{\partial g}{\partial y_s}y_{s+1}\right) \equiv f(y_n, y_{n-1}, ...y, x). \tag{B2}$$

If the function f is nonlinear in y_n, take a second derivative to obtain

$$\frac{\mathrm{d}y_{n+1}}{\mathrm{d}x} = \kappa y_{n+1} - Q_2, \tag{B3}$$

where

$$\kappa \equiv \frac{\partial f}{\partial y_n} \tag{B4}$$

and

$$Q_2 \equiv -\frac{\partial f}{\partial x} - \sum_{s=0}^{n-1}\frac{\partial f}{\partial y_s}y_{s+1}. \tag{B5}$$

Equation (B3) is linear in y_{n+1} as claimed, because κ and Q_2 do not depend on y_{n+1}. Unlike equation (24), however, (B3) is a first-order differential equation. It therefore has different stability properties, and κ has units of x^{-1} rather than x^{-2}.

The present scheme usually requires one more derivative than Newton's method for finding roots [32], but the final equations are linear. Stability is therefore easier to assess, and semi-implicit schemes often work well independent of the sign of κ. Solutions for $y(x)$ can thus be obtained quickly and easily for many problems.

References

[1] Sudit I and Woods R C 1994 *J. Appl. Phys.* **76** 4488
[2] Hoskinson A R and Hershkowitz N 2006 *Plasma Sources Sci. Technol.* **15** 85
[3] Chen F F 2001 *Phys. Plasmas* **8** 3029
[4] Godyak V A, Piejak R B and Alexandrov B M 1993 *J. Appl. Phys.* **73** 3657
[5] Shih C H and Levi E 1971 *AIAA J.* **9** 1673
[6] Annaratone B M, Allen M W and Allen J E 1992 *J. Phys. D: Appl. Phys.* **25** 417
[7] Lee D and Hershkowitz N 2007 *Phys. Plasmas* **14** 033507
[8] Chen F F, Etievant C and Mosher D 1968 *Phys. Fluids* **11** 811
[9] Steinbrüchel C 1990 *J. Vac. Sci. Technol.* A **8** 1663
[10] Laframboise J G 1966 *Report 100* Institute for Aerospace Studies, University of Toronto
[11] Laframboise J G and Parker L W 1973 *Phys. Fluids* **16** 629
[12] Chen F F 1965 *J. Nucl. Energy* C **7** 47
[13] Allen J E 1992 *Phys. Scr.* **45** 497
[14] Karamecheti A and Steinbrüchel C 1999 *J. Vac. Sci. Technol.* A **17** 3051
[15] Sheridan T E 2000 *Phys. Plasmas* **7** 3084
[16] Hershkowitz N 1989 *Plasma Diagnostics* vol 1, ed O Auciello and D L Flamm (London: Academic) p 113
[17] Amemiya H, Annaratone B M and Allen J E 1999 *Plasma Sources Sci. Technol.* **8** 179
[18] Allen J E, Boyd R L F and Reynolds P 1957 *Proc. Phys. Soc.* **70** 297
[19] Bernstein I B and Rabinowitz I N 1959 *Phys. Fluids* **2** 112
[20] Fernsler R 2007 *Bull. Am. Phys. Soc.* **52** 69
[21] Benilov M S, Bochkarev G G and Rogov B V 1995 *IEEE Trans. Plasma Sci.* **23** 742

[22] Kono A 2003 *Phys. Plasmas* **10** 4181
[23] Fernsler R F, Slinker S P and Joyce G 2005 *Phys. Rev.* E **71** 026401
[24] Riemann K-U 1995 *IEEE Trans. Plasma Sci.* **23** 709
[25] Riemann K-U 1991 *J. Phys. D: Appl. Phys.* **24** 493
[26] Kennedy R V and Allen J E 2002 *J. Plasma Phys.* **67** 243
[27] Stangeby P C and Allen J E 1971 *J. Plasma Phys.* **6** 19
[28] Riemann K-U 2004 *IEEE Trans. Plasma Sci.* **32** 2265
[29] Sternberg N and Godyak V 2003 *IEEE Trans. Plasma Sci.* **31** 665
[30] Franklin R N 2003 *Phys. Plasmas* **10** 4589
[31] Lam S H 1965 *Phys. Fluids* **8** 73
[32] Conte S D 1965 *Elementary Numerical Analysis* (New York: McGraw-Hill) p 30